Thermodynamic Assessment of an Integrated PDSC–TES–AMTEC–TEG Solar Micro-CHP System

Ahmed Faeq Mohammed
Department of Mechanical Engineering, Engineering Faculty, Urmia University, Urmia, Iran
Email: ahmed.fmh26@gmail.com

Article History

Received: Mar. 24, 2026

Revised: Jul. 12, 2026

Accepted: Jul. 29, 2026

Abstract

Decentralized renewable energy systems that generate electricity as well as useful heat have been gaining more attention as efficient alternatives to traditional fossil-fuel energy systems. This study reports a thermodynamic analysis of a solid-state solar micro-combined heat and power (mCHP) system that uses an alkali metal thermal-to-electric converter, latent thermal energy storage, a thermoelectric generator, and a parabolic dish solar concentrator. The configuration is designed to optimize solar energy use, integrating high-temperature solar heat collection, thermal storage, direct thermal-to-electric conversion, and waste heat recovery into a compact and modular system. The performance of the integrated system was analyzed using the methods of energy and exergy analysis, and the main sources of irreversibilities were identified. Suitable operating conditions were investigated by studying the effects of the key operating parameters such as receiver wall temperature, AMTEC current, condenser temperature, and TEG current. The results indicate that the proposed system can produce a total electrical power of 7372 W, including 6241 W from the AMTEC and 1131 W from the TEG, as well as useful heating power of 8242 W at 80 °C. The efficiencies for electrical and overall CHP are 24.75% and 52.05%, respectively. Moreover, the electrical exergy efficiency and overall exergy efficiency are 26.4% and 31.01%, respectively, and the overall rate of exergy destruction is 19231 W. From the exergy analysis it is seen that the solar collection stage is the largest source of irreversibility. The proposed PDSC–TES–AMTEC–TEG system has good potential for use as a dependable, modular, and fully solid-state solar micro-CHP system for decentralized energy applications.

Keywords- Alkali metal thermal-to-electric converter, Micro-combined heat and power, Parabolic dish solar concentrator, Thermal energy storage, Thermoelectric generator.

I. INTRODUCTION

Significant challenges, such as growing energy demand, environmental issues, and the need for greenhouse gas reductions, confront the world's energy industry. Traditionally fossil fuels have been the primary energy source, but their large consumption has caused serious issues with climate change, air pollution, and energy security. As a result, the world has prioritized the transition to sustainable, reliable, and low-carbon energy systems. Solar energy is one of the most promising renewable energy sources due to its abundance, availability, and use in both decentralized and centralized energy systems. Although PV systems have been experiencing rapid growth, solar thermal technologies, such as Concentrating Solar Power (CSP), have the potential to greatly benefit from the ability to store the heat generated by high-temperature devices when needed.

The capabilities of integration with Thermal Energy Storage (TES) make CSP systems particularly appealing, as it allows for a more consistent and controllable supply of energy. On the other hand, the conventional CSP plants are mostly built at large sizes, have higher capital costs, and need high direct normal irradiance (DNI) and complex infrastructure. These constraints have fueled interest in CSP with small-scale and compact configurations for decentralized and off-grid applications. The modular structure, high operating temperature, and high concentration ratio make parabolic dish concentrators particularly suitable for small-scale systems among the CSP technologies. These properties render them as having excellent potential for combination with advanced thermal-to-electric conversion technologies like Alkali Metal Thermal-to-Electric Converters (AMTECs) and Thermoelectric Generators (TEGs). AMTEC can be directly used to generate electricity at high temperatures, while TEGs can recover the residual heat and enhance the energy utilization of the whole system.

However, effective thermal storage is needed for such solar thermal systems to operate on a continuous basis. During sunny days, TES can store excess energy from the sun and, on cloudy days, release the stored heat to provide a continuous power and heat supply, thus enhancing the reliability of the solar power. Hence, a combination of parabolic dish CSP, AMTEC, TEG, and TES could be a potential way to realize the compact micro-CHP based on solar energy. In this context, the current study focuses on a small-scale hybrid solar thermal system that utilizes a parabolic dish concentrator, AMTEC, TEGs, and thermal energy storage. The primary goal is to test the feasibility of this combined system for sustainable electricity and useful heat production, especially in decentralized, remote, and off-grid settings.

This section covers a review of the previous studies and the key technologies used in the solar thermal energy system, focusing on the concentrating solar power technologies, parabolic dish concentrator technologies, alkali metal thermal-electrical converter technologies, thermal energy storage technologies, and thermoelectric generator technologies.

Although parabolic-trough systems remain the dominant system for existing CSP installations, most new deployments are using tower systems, as suggested by Alami et al. [1]. The change indicates a growing interest in the sector of increasing receiver temperatures and integrating thermal energy storage. One of the main benefits of CSP is that it offers not only power but also high-temperature heat. This allows CSP to be especially useful in industrial applications and for dispatchable, nighttime, or cloudy day power generation, which conventional PV systems cannot offer without storage. In the review by Wu et al. [2], concentrated solar thermal power technologies were reviewed, as well as their applications in thermal energy uses for industry. They demonstrated the use of solar thermal technology for the generation of process heat in the range of 150 °C to more than 500 °C for steam generation, desalination, process heating, and combined heat and power applications. Their findings demonstrated that parabolic troughs can achieve 80% efficiency, while solar tower systems are more appropriate for extensive applications exceeding 1000°C. They also have LCOE values of 60-100 USD·MWh^{-1}; however, these systems still face high capital costs and integration challenges that hinder widespread implementation. In the study conducted by Çakır et al. [3], they investigated the main CSP technologies, such as solar towers, parabolic trough collectors, dish-Stirling systems, and linear Fresnel reflectors. The authors pointed out the potential of thermal energy storage to store high-temperature heat and provide dispatchable power in the CSP system. They analyzed the pros and cons of various configurations and observed that further refinements in the heat-transfer fluid, tracking systems, and AI-driven control strategies are likely to further improve CSP performance and reliability. Parabolic dish concentrators are also becoming more popular as a type of CSP for small and decentralized uses because they have a high concentration ratio, take up less space, and can be built in modules. García-Ferrero et al. [4] have conducted a review of parabolic dish concentrators, focusing on various subsystems, integration methods, and system optimization. Parabolic dish collectors can be used to produce high operating temperatures due to the ability to focus solar energy into a small receiver area, they reported. The authors highlighted that parabolic dish concentrators are suitable for small-scale electricity and heat generation in remote areas, either as standalone units or as arrays of dishes. They pointed out, however, that the parabolic dish concentrators are still one of the least advanced CSP technologies, which means that there is a need for further development of systems integrated with and optimized for a parabolic dish. Kumar et al. [5] have studied the performance of parabolic dishes for different geometries of the receiver and investigated the influence of different heat transfer media. They found that conical or hemispherical receiver cavities achieve a combined optical and thermal performance improvement of 8%-12%. They also found that metal oxide nanofluids as a heat transfer medium improved heat transfer and boosted the overall efficiency by 10 to 13%. The results indicate that the use of the receiver design and the selection of the heat-transfer fluid are important to enhance the performance of dish-based CSP systems. Another important technology that can enhance the dispatchability and reliability of solar thermal energy is thermal energy storage. A review of 56 studies by Esfanjani et al. [6] reported that most of the studies conducted on dish system integration for PCM are simulation-based. The small number of experimental results that are available, however, showed 5–13% improvements in efficiency and a 20% reduction in the time to boil when short-term PCM buffering was employed to reduce the solar transients. They emphasized the importance of prototypes of the dish that can be used above 800 K and can reduce the need for the control of the heat-transfer fluid.

Opolot et al. [7] discussed the properties of the HTPCMs with a melting point of more than 500 °C and concluded that the aluminum-silicon alloys with a eutectic melting point near 577 °C, magnesium-silicon mixtures, and chloride salts are excellent candidates. The latent heats of these materials range from 350 to 550 kJ·kg^{-1}. But they still present significant technical challenges in their practical application for high-temperature thermal energy storage (HT-TES) due to low thermal conductivity and unknown corrosion behavior. Wang et al. [8] discussed the characteristics of different kinds of thermal energy storage media and found that nitrate salts are widely used due to their moderate temperature stability and chemical stability. They do start to decompose above 565°C and start to solidify around 220°C, which restricts them from being used in high-temperature CSP applications. The high thermal conductivity, around 84 W·m^{-1}·K^{-1}, and low viscosity of liquid sodium proved to be an attractive option for use at high operating temperatures above 700°C. Li et al. [9] created a dynamic model that is fully coupled between a 100 MWe heliostat field, a sodium receiver, three different forms of the TES, and a recompression supercritical Brayton cycle. They considered two types of packed-bed systems: one filled with solid filler (PBS-TES) and another with packed capsules of PCM (PBP-TES), which are filled with chloride salts, and compared both with a conventional two-tank molten-salt system. The average daily efficiency slightly decreased for the alternative designs from 26.0% for PBS-TES to 25.5% for PBP-TES. But they made significant savings in the space required and the costs of materials. The costs were cut by 42% and 21% with PBS-TES and PBP-TES, respectively, reducing the size of the TES by 64% and 83%. Kee et al. [10]

expanded sodium-based storage and conversion concepts to a 1 MWe tower system with sodium boiling directly in the receiver and thermal energy stored through NaCl phase change. Their design, optimised for 14-hour storage, projected an LCOE of 128 USD·MWh^{-1}. This value was competitive for microgrid applications and 15% lower than that of a 100 MWe molten-salt reference system on a per-kilowatt basis. This study shows the potential of sodium-based CSP systems for smaller and more flexible power generation applications. In addition to thermal storage, advanced direct thermal-to-electric conversion technologies can improve the overall efficiency of solar thermal systems. Tohidi et al. [11] reviewed state-of-the-art thermoelectric materials for mid-temperature operation. They reported that Bi-Te alloys, skutterudites, and half-Heusler compounds can achieve ZT values between 1.5 and 2.0, while bulk SnSe has demonstrated a record ZT of 3.1 near 780 K. These values correspond to realistic thermoelectric generator efficiencies between 11% and 17% in the 550–700 K range, which is well matched to AMTEC condenser temperatures.

Peng et al. [12] developed an analytical model of a solar-driven AMTEC system that incorporated losses in the solar collector, vapour loop, and AMTEC cell. Their results emphasized the trade-off between power density and efficiency. A BASE membrane thickness of 150 μm operated at 1.2 A·cm^{-2} maximized specific power, while a thinner 90 μm membrane improved efficiency up to approximately 29% at the cost of increased sealing stress. The study also introduced an area-ratio criterion for matching absorber area to BASE area, suggesting an optimal range between 1.6 and 1.9. Tohidi et al. [13] thermally bonded a 128-cell sodium AMTEC to a SnSe-based TEG array through a high-conductivity metal–ceramic laminate. This direct attachment minimized the temperature drop across the interface to approximately 1 K. With co-optimization of current density, thermoelectric leg geometry, and module count, they increased net electrical output from 6.7 kW to 11.2 kW and improved system efficiency from 30.7% to 38.9%. Their work also demonstrated that power output could be modulated by ±10% with less than two percentage points of efficiency loss, provided that the condenser temperature was maintained between 580 and 700 K. Peng et al. [14] developed a two-stage Na-TEC unit followed by a segmented-leg TEG. By co-optimizing the condenser temperature, approximately 630 K, and TEG current density, they increased system efficiency from 36% to 41.3% and raised the specific power by 67%, achieving 68.7 kW·m^{-2}. This benchmark remains an important reference point for subsequent hybrid thermal-to-electric conversion systems across solar, fuel-cell, and nuclear applications.

Zhao et al. [15] added a thermally regenerative electrochemical cycle and a final TEG to a high-flux AMTEC system. Under 200-sun illumination, their three-stage cascade improved efficiency by 28.6% and increased power density by nearly 50% compared with a stand-alone AMTEC. This study further confirms the potential of cascade systems for energy conversion to extract additional useful work from residual heat. Overall, previous studies have confirmed the potential of CSP technologies for dispatchable power generation and high-temperature heat supply. Parabolic dish systems are particularly attractive for small-scale, decentralized applications because of their high concentration ratio, modularity, and compact structure. In parallel, advances in TES, AMTEC, and TEG technologies have shown that thermal storage and cascade energy conversion can significantly improve system continuity and overall efficiency.

However, important research gaps remain. Most existing studies focus on large-scale CSP configurations or the independent optimization of individual subsystems. In addition, dish-scale TES investigations are still largely simulation-based, and limited attention has been given to the integrated operation of parabolic dish concentrators with high-temperature TES, AMTEC, and TEGs in a compact system. Therefore, this study investigates a small-scale, hybrid solar thermal configuration that combines these technologies to evaluate their potential for continuous electricity generation and useful heat production in decentralized and off-grid applications.

II. SYSTEM DESCRIPTION

The proposed system is a solar-driven micro combined heat and power (micro-CHP) system comprising a parabolic dish solar concentrator (PDSC), thermal energy storage (TES), an alkali metal thermal-to-electric converter (AMTEC), and a thermoelectric generator (TEG). The goal is to provide both electricity and useful heat in a decentralized and small-scale manner and to maximize the number of operating hours in the face of varying solar conditions through high solar concentration with efficient thermal conversion and storage.

The direct normal irradiance is focused on a cavity receiver by a two-axis tracking PDSC, as illustrated in Figure 1. Sodium (Na) is used as HTF (heat transfer fluid) and working fluid. In the receiver, the sodium is heated and evaporated at a nominal temperature of ~1200 K. The vaporized sodium flows through the flow control valve and is directed to the AMTEC subsystem, where high-temperature thermal energy is directly converted to electricity via electrochemical processes. Various thermoelectric generator (TEG) modules are installed on the walls of the condenser to recover the mid-temperature residual heat ($T_{cond} \approx 600–700$ K). This cascaded system would have higher energy utilization, as it would produce extra power from the waste heat. The cold side of the TEG modules is thermally coupled to a water-cooled heat exchanger with an operating temperature of about 353.15 K. The rejected heat is utilized as useful hot water, which adds to the CHP output. During normal solar operation, the condensed sodium is recirculated to the receiver. In TES-assisted operation, the sodium stream flows through the TES heat exchanger, where the thermal energy stored in the TES is transferred to the working fluid before it re-enters the AMTEC loop. At the same time, the overflow of the sodium vapor, which is not fed to the AMTEC, is channeled to the TES subsystem for charging. Potassium carbonate (K_2CO_3) is used as a phase-change material (PCM) in the TES. The high-temperature sodium vapor entering the TES heat exchanger condenses, transferring the

latent and sensible heat to the PCM to melt. Thus, high-temperature thermal energy is stored and can be extracted when the solar input is not adequate (e.g., during cloud transients or as a night store). The integration of the PDSC, TES, AMTEC, and TEG results in a modular micro-CHP system that generates electrical power and useful thermal energy more reliably and with higher energy efficiency.
From a practical implementation perspective, the use of potassium carbonate (K2CO3) as a high-temperature phase-change material (PCM) and liquid sodium as the heat transfer fluid introduces compatibility and containment challenges. At operating temperatures around 1170 K, molten salts can accelerate chemical degradation and corrosion on storage vessel walls, heat exchanger surfaces, and structural joints, particularly under cyclic thermal loading. Similarly, liquid sodium requires highly reliable containment materials due to its reactivity at elevated temperatures. Addressing these corrosion mechanisms and selecting suitable alloys (such as nickel-based superalloys or specialized stainless steels) are critical for ensuring system longevity and should be systematically investigated in future experimental assessments.

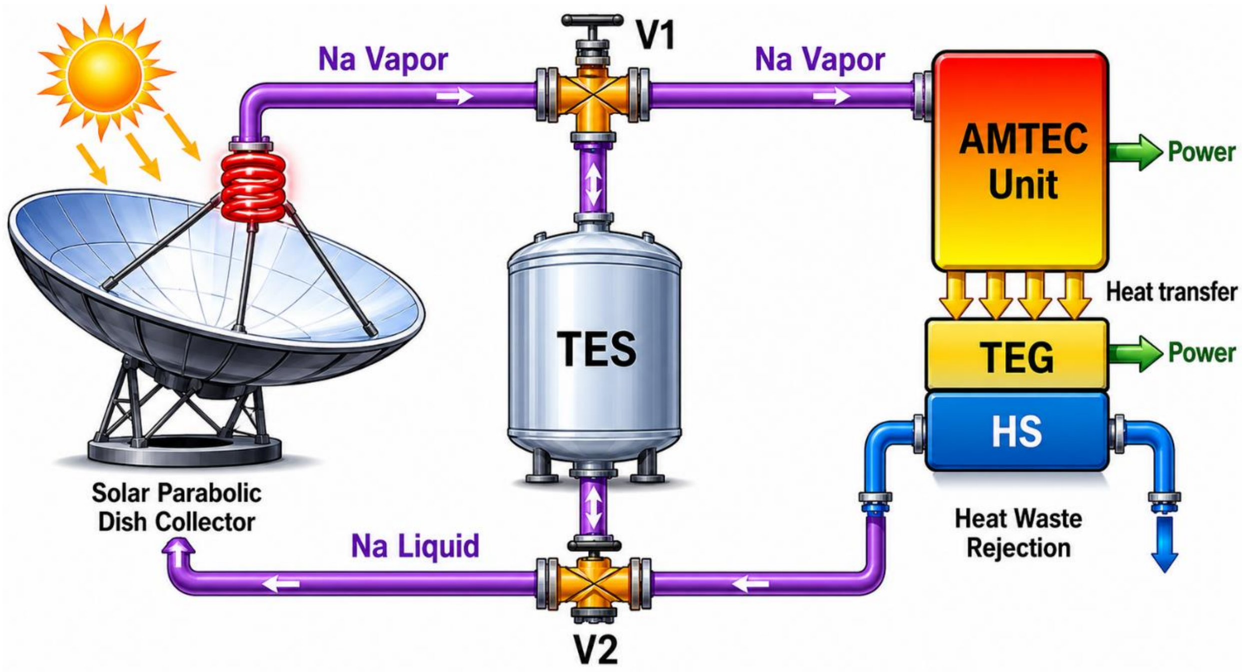

Figure 1. Schematic diagram of the proposed solar-driven micro-CHP system.

III. THERMODYNAMIC MODELING

The thermodynamic model of the proposed micro-CHP system (PDSC–TES–AMTEC–TEG) is developed using the 1st and 2nd laws of thermodynamics. The model is used to assess useful thermal energy from the parabolic dish solar concentrator, the charging and discharging performance of the thermal energy storage unit, the electrical power from the AMTEC and TEG subsystems, and the overall energy and exergy performance of the integrated system.

- **Assumptions**

The thermodynamic analysis is based on the following general assumptions:

1. The PDSC, AMTEC, and TEG subsystems are assumed to operate at steady state during each selected operating condition, whereas the TES is represented through separate charging and discharging modes under a quasi-steady-state approach.
2. Direct normal irradiance is considered the solar input to the parabolic dish solar concentrator.
3. A comprehensive loss term accounts for the heat losses from the receiver and storage tank.
4. During the charging period, excess heat is stored in the TES unit, and during the discharge period, heat is supplied to the AMTEC.
5. The heat rejected from the AMTEC condenser is recovered by the TEG subsystem.
6. The heat left after the TEG is used as the useful heat produced by the micro-CHP system.
7. The changes in kinetic energy and potential energy are neglected.
8. Ambient temperature is used to represent the reference temperature in an exergy analysis.

- **Parabolic Dish Solar Concentrator Model**

A parabolic dish solar concentrator (PDSC) is used to convert direct normal irradiance into high-temperature thermal energy at the receiver. The incident solar power on the concentrator aperture is

$$\dot{Q}_{Solar} = DNI\, A_{con} \quad (1)$$

where DNI is the direct normal irradiance and A_{con} is the aperture area of the concentrator. The absorbed solar power by the receiver is expressed as:

$$\dot{Q}_{Rec} = \eta_o\, \dot{Q}_{Solar} \quad (2)$$

where η_o is the optical efficiency of the concentrator-receiver system. Useful heat received is the difference between the absorbed solar power and total thermal losses from the receiver:

$$\dot{Q}_{Use} = \dot{Q}_{Rec} - \dot{Q}_{Loss} \quad (3)$$

The first-law efficiency of the PDSC is defined as:

$$\eta_I^{PDSC} = \frac{\dot{Q}_{Use}}{\dot{Q}_{Solar}} \quad (4)$$

For the second-law analysis, the exergy input due to solar radiation is calculated by applying the Petela relation:

$$\dot{Ex}_{in}^{PDSC} = \dot{Q}_{Solar}\left[1 - \frac{4}{3}\left(\frac{T_{Ref}}{T_{sun}}\right) + \frac{1}{3}\left(\frac{T_{Ref}}{T_{sun}}\right)^4\right] \quad (5)$$

The useful exergy yield of the PDSC is:

$$\dot{Ex}_{out}^{PDSC} = \dot{Q}_{Use}\left(1 - \frac{T_{Ref}}{T_W}\right) \quad (6)$$

- **Thermal Energy Storage Model**

Since the TES charging and discharging processes are inherently transient, they are represented here by separate quasi-steady operating modes. The present model estimates the stored and discharged energy without resolving the detailed time-dependent evolution of the PCM state. There is a thermal energy storage (TES) unit that stores excess thermal energy from the PDSC and can provide energy to the AMTEC when the solar radiation is inadequate. The rate at which the TES charges is given by:

$$\dot{Q}_{Charge}^{TES} = \dot{Q}_{Use} - \dot{Q}_{In}^{AM} \quad (7)$$

For the present quasi-steady formulation, the maximum latent thermal energy that can be stored in the TES is calculated from the PCM mass and its latent heat of fusion:

$$Q_{Charge}^{TES} = M_{PCM}\, h_{SF,PCM} \quad (8)$$

The total thermal energy delivered from the TES during a prescribed discharging period is calculated as:

$$Q_{Discharge}^{TES} = \dot{Q}_{Discharge}^{TES}\, t_{discharge} \quad (9)$$

The energy efficiency of the TES subsystem is represented as:

$$\eta_I^{TES} = \frac{Q_{Discharge}^{TES}}{Q_{Charge}^{TES}} \quad (10)$$

The TES exergy efficiency is defined as:

$$\eta_{II}^{TES} = \frac{Ex_{Discharge}^{TES}}{Ex_{Charge}^{TES}} \quad (11)$$

- **AMTEC Model**

Alkali metal thermal-to-electric converter (AMTEC) is a device that converts high-temperature thermal energy into electrical power that is based on sodium as the working fluid. In the suggested system, the heat can be provided directly to the AMTEC or during discharge to the TES. The electrical power produced by the AMTEC is:

$$P_{AM} = V_{AM}^{eff}\, I_{AM} \quad (12)$$

The energy efficiency of the AMTEC is defined as:

$$\eta_I^{AM} = \frac{P_{AM}}{\dot{Q}_{In}^{AM}} \quad (13)$$

The heat rejected from the AMTEC condenser is recovered by the TEG subsystem:

$$\dot{Q}_{Out}^{AM} = \dot{Q}_{In}^{AM} - P_{AM} \quad (14)$$

The AMTEC subsystem exergy destruction rate is given as:

$$\dot{Ex}_D^{AM} = \dot{Ex}_{In}^{AM} - P_{AM} - \dot{Ex}_{Out}^{AM} \qquad (15)$$

- **Thermoelectric Generator Model**

The thermoelectric generator (TEG) is a device that extracts the heat that is rejected from the AMTEC condenser and uses some of it to generate extra electricity. Hence, the heat input for the TEG is:

$$\dot{Q}_{in}^{TEG} = \dot{Q}_{Out}^{AM} \qquad (16)$$

The electrical power produced by the TEG is:

$$P_{TEG} = \eta_{TEG}\, \dot{Q}_{in}^{TEG} \qquad (17)$$

The value of the remaining heat after the TEG is taken as the useful heat output of the micro-CHP system:

$$\dot{Q}_{Heating} = \dot{Q}_{in}^{TEG} - P_{TEG} \qquad (18)$$

The useful heating rate can also be correlated to the temperature increase of the water as follows:

$$\dot{Q}_{Heating} = \dot{m}_w\, c_{p,w} \left(T_{w,out} - T_{w,in}\right) \qquad (19)$$

- **Overall System Performance**

The overall electrical power generation of the proposed micro-CHP system is the sum of the power generation of the AMTEC and TEG:

$$P_{Sys} = P_{AM} + P_{TEG} \qquad (20)$$

The overall electrical efficiency is given by:

$$\eta_{I,Sys}^{Elec} = \frac{P_{Sys}}{\dot{Q}_{Solar}} \qquad (21)$$

The overall CHP efficiency, including both electrical power and useful heating output, is:

$$\eta_{I,Sys}^{CHP} = \frac{P_{Sys} + \dot{Q}_{Heating}}{\dot{Q}_{Solar}} \qquad (22)$$

The exergy associated with the useful heating output is:

$$\dot{Ex}_{Heating} = \dot{Q}_{Heating} \left(1 - \frac{T_{Ref}}{T_{Heating}}\right) \qquad (23)$$

The overall CHP exergy efficiency is defined as:

$$\eta_{II,Sys}^{CHP} = \frac{P_{Sys} + \dot{Ex}_{Heating}}{\dot{Ex}_{in}^{PDSC}} \qquad (24)$$

Finally, the total exergy destruction rate of the integrated system is calculated as:

$$\dot{Ex}_D^{Sys} = \dot{Ex}_D^{PDSC} + \dot{Ex}_D^{TES} + \dot{Ex}_D^{AM} + \dot{Ex}_D^{TEG} \qquad (25)$$

The matching of these indicators is used to assess the electrical, thermal, and exergetic performance of the integrated PDSC–TES–AMTEC–TEG micro-CHP system.

IV. MODEL VALIDATION

The developed models were validated with the reliable data acquired from literature before carrying out parametric and system-level studies. As illustrated in Figure 2, the PDSC model was compared with the collector efficiency data reported by Wu et al. [16], and good agreement was obtained over the investigated receiver-temperature range. The AMTEC model was checked for the benchmark model of Tournier and El-Genk [17] in Table 1, and the differences were found to be less than 2.5% in first-law efficiency and within ±4.1% in power output. Moreover, Table 2 compares the experimental data of Liao et al. [18] with the results of the TEG model, showing maximum deviations of approximately 8% in power output and 6% in open-circuit voltage. The agreement shows that the developed models are able to accurately predict the performance of the main subsystems and can be used to perform an integrated system performance evaluation.

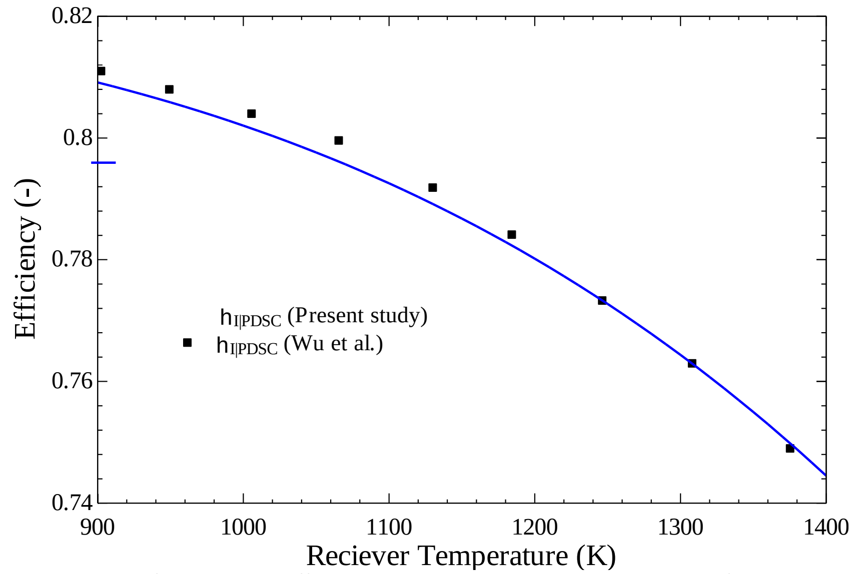

Figure 2. Validation of overall PDSC efficiency versus receiver temperature with results from Wu et al. [16].

Table 1 .Validation of AMTEC model predictions against data from Tournier and El-Genk [17].

I_{AM} (A)	η_I^{AM} (%) (Ref [17])	η_I^{AM} (%) (Present Model)	Rel. Err (%)	P_{AM} (W) (Ref [17])	P_{AM} (W) (Present Model)	Rel. Err (%)
20	28.3	27.82	–1.70	1703	1634	–4.05
46	30.6	29.91	–2.25	3340	3294	–1.38
81	29.1	28.38	–2.47	5125	5043	–1.60
121	25.9	25.34	–2.16	6260	6179	–1.29
169	21.7	21.22	–2.21	6730	6637	–1.38

Table 2. Validation of TEG model predictions against experimental data from Liao et al. [18].

T_h(K)	P_{TE}(W) (Ref.[18])	P_{TE}(W) (Present Model)	Rel. Err. (%)	$V_{TE,oc}$ (V) (Ref.[18])	$V_{TE,oc}$ (V) (Present Model)	Rel. Err. (%)
313	0.017	0.0181	+6.47	0.45	0.428	–4.89
323	0.070	0.0728	+4.00	0.90	0.873	–3.00
333	0.170	0.1633	–3.94	1.40	1.327	–5.21
373	0.950	0.875	–7.89	3.40	3.208	–5.65
413	2.200	2.074	–5.73	5.35	5.146	–3.81
453	3.850	3.707	–3.71	7.20	7.097	–1.43

493	5.580	5.662	+1.47	8.85	8.989	+1.57

V. PARAMETRIC ANALYSIS AND DISCUSSION

The assumptions and operating parameters in Table 3 were used for the parametric analysis. Only one parameter was changed at a time in each analysis, and the others were fixed at their reference values. The goal was to identify the major thermodynamic and electrochemical compromises between the PDSC, TES, AMTEC, and TEG subsystems and to provide a set of operating conditions for the integrated micro-CHP system.

Table 3. Baseline assumptions and operating parameters used in the parametric analysis.

Subsystem	Parameter	Symbol	Value	Unit	Ref.
PDSC	Direct normal irradiance	DNI	900	$W\cdot m^{-2}$	[5], [16]
	Dish aperture area	A_{con}	100	m^2	[5], [16]
	Aspect ratio	HD_{ratio}	0.25	–	[5], [16]
	Rim angle	ϕ_{rim}	45	°	[5], [16]
	Mirror reflectivity	ρ_{mirror}	0.94	–	[5], [16]
	Receiver absorptance	α_{rec}	0.95	–	[5], [16]
	Air-path transmittance	τ_{air}	0.98	–	[5], [16]
	Window transmittance	τ_{window}	0.96	–	[5], [16]
	Intercept factor	$c_{intercept}$	0.99	–	[5], [16]
	Un-shading factor	$k_{unshade}$	0.99	–	[5], [16]
	Cavity wall emissivity	ε_c	0.90	–	[5], [16]
TES	Latent heat of fusion	$h_{SF,PCM}$	235.8	$kJ\cdot kg^{-1}$	[7], [19]
	Melting temperature	$T_{M,PCM}$	1170	K	[7], [19]
	PCM density	ρ_{PCM}	2290	$kg\cdot m^{-3}$	[7], [19]
	Overall heat loss coefficient	U_{TES}	0.5	$W\cdot m^{-2}\cdot K^{-1}$	[7], [19]
	Aspect ratio	D_{TES}/L_{TES}	2	–	[7], [19]
AMTEC	BASE thickness	D_B	200	μm	[17], [20], [21]
	Electrode area in each BASE element	A_E	140.8	cm^2	[17], [20], [21]
	Charge exchange coefficient	B_{AM}	90	$A\cdot K^{1/2}\cdot Pa^{-1}\cdot m^{-2}$	[17], [20], [21]
	BASE electrical contact resistance	$R'_{B,cont}$	0.1	$\Omega\cdot cm^2$	[17], [20], [21]
	Electrode volumetric porosity	ε_E	0.9	–	[17], [20], [21]
	Effective emissivity of BASE	ε_B	0.9	–	[17], [20], [21]
	Effective emissivity of condenser	ε_{cond}	0.02	–	[17], [20], [21]
	Number of radiation shield layers	n	8	–	[17], [20], [21]
	Radiation shield effective emissivity	ε_s	0.3	–	[17], [20], [21]

TEG	Surface area of each TEM	$A_{ceramic}$	40 × 40	mm²	[22]
	Ceramic cover thickness	$D_{ceramic}$	0.86	mm	[22]
	Ceramic cover thermal conductivity	$\lambda_{ceramic}$	36	W·m⁻¹·K⁻¹	[22]
	Number of uncouples in each TEM	N_{TE}	127	–	[22]
	Surface area of n-type thermoelectric leg	A_n	2.6 × 2.6	mm²	[22]
	Electrical contact resistance	r^c	1×10^{-5}	Ω·cm²	[22]

- **Effect of receiver wall temperature**

One of the most important parameters in the integrated system is the wall temperature of the receiver, T_W, which influences the performance of the solar receiver as well as the working condition of the TES and AMTEC subsystems. From the results shown in Figure 3, it can be seen that the energy and exergy efficiency of the TES decrease with the increase in T_W. This phenomenon is primarily because of the greater temperature difference between the storage medium and the ambient temperature, resulting in a greater thermal loss from the TES. The AMTEC efficiency, on the other hand, increases as the T_W increases. BASE temperature increases the vapor pressure of the sodium vapors on the anode side and enhances the electrochemical driving force for better AMTEC power conversion.

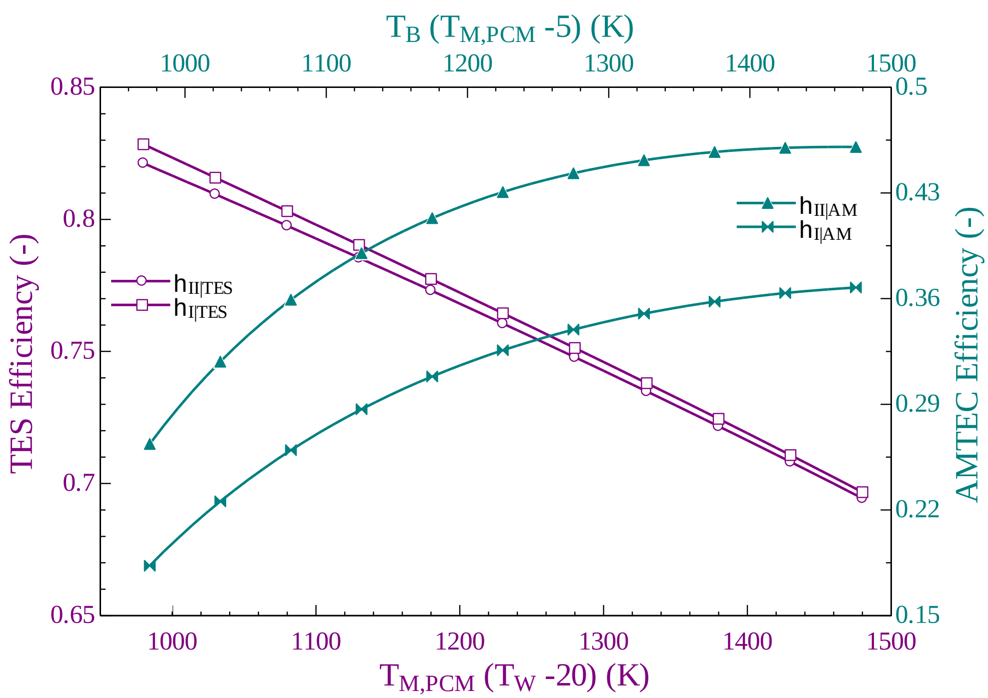

Figure 3. Effect of T_W on the energy and exergy efficiencies of TES and AMTEC subsystems.

The overall system response to T_W, as shown in Figure 4, is almost identical. The total electrical power increases with T_W up until approximately 1300 K, after which it begins to decline. This is because the AMTEC performs better at higher temperatures, but less heat is available for downstream recovery and TEG conversion. As the T_W rises, the recovered heating decreases due to the fact that more of the available thermal energy is converted to electric power in the AMTEC, and less heat is available for recovery at the TEG outlet. The lower the CHP energy efficiency, the higher the T_W, as the increase in electrical power does not make up for the decrease in recovered heat. On the other hand, the exergy efficiency of the CHP first improves and then declines, peaking at around 1220 K. The interval of 1220–1300 K can be considered the optimum working range because, in this interval, both the maximum electrical output and maximum exergy efficiency of the process are achieved. Based on this study, 1220 K has been selected as the recommended value due to a balance that is achieved between the electrical generation, heat recovery, and overall exergy efficiency.

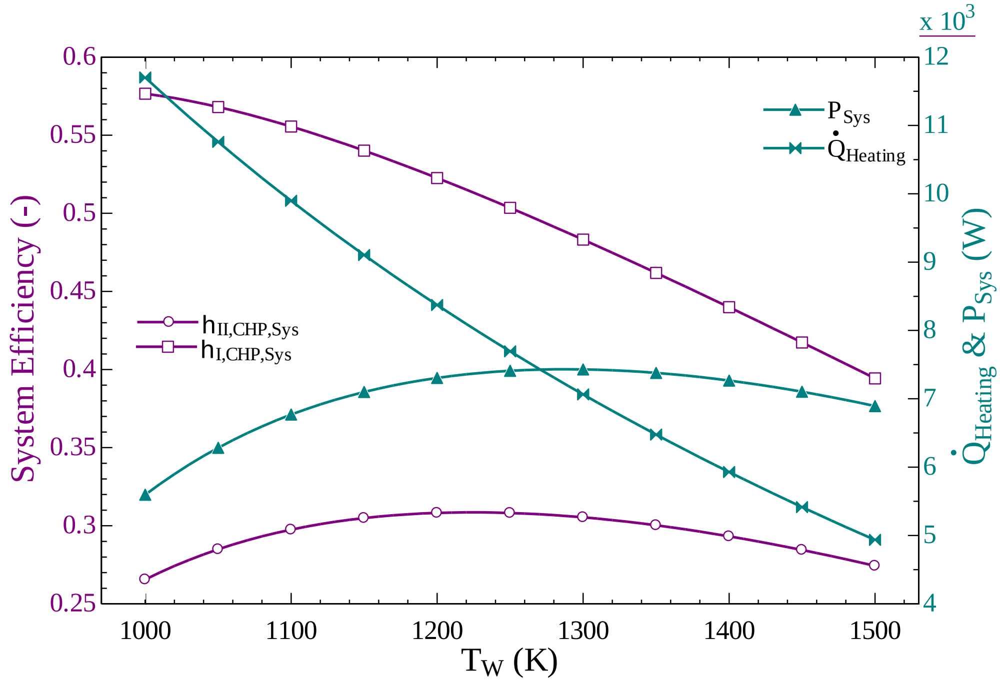

Figure 4 .Behavior of system heat and power generation and energy and exergy efficiency with receiver wall temperature.

- **Effect of AMTEC current**

The AMTEC current, I_{AM}, affects the AMTEC voltage, power output, internal losses, and number of BASE elements. Thus, it makes a significant impact on the performance of the subsystems and systems. The energy and exergy efficiencies of the AMTEC are seen to rise with decreasing current, peak around 50 A, and drop with further increases in current, as shown in Figure 5. The higher the number of BASE elements, the larger the radiative heat transfer area and the greater the thermal losses at low currents. The higher the current, the fewer the number of required base elements and the smaller the radiation losses, making the process more efficient. However, outside the optimum range, ohmic losses and polarization losses are predominant. These voltage losses will decrease the net electrochemical output of the AMTEC, leading to a reduction in power generation and efficiency. Hence, the AMTEC displays a clear optimum current on the basis of the standalone conversion performance.

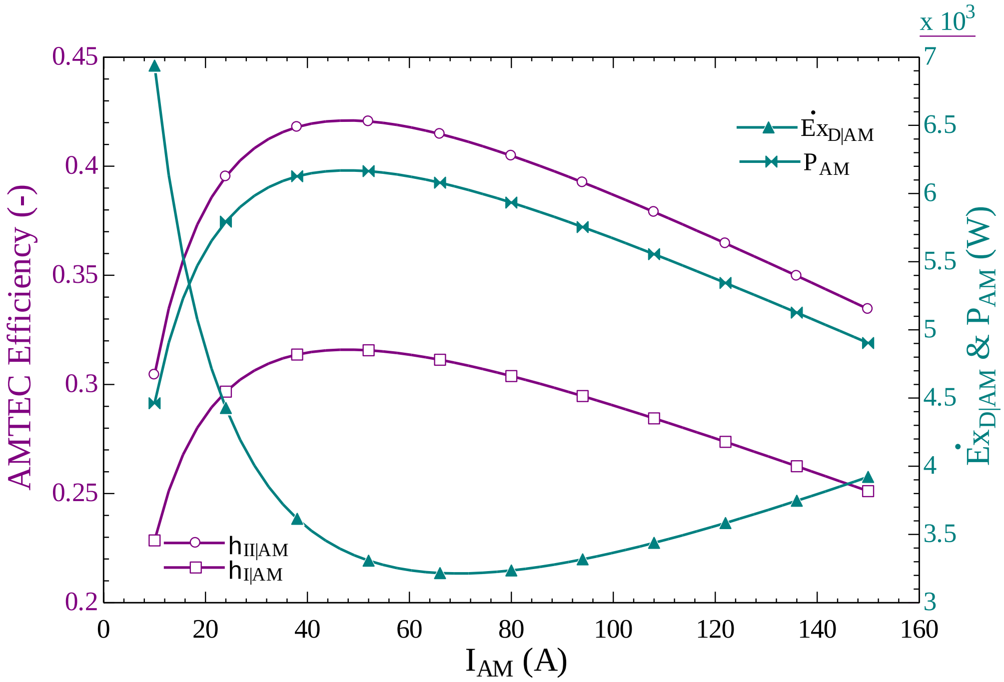

Figure 5. Influence of AMTEC current on energy and exergy efficiency of the AMTEC unit and also its power generation and exergy destruction.

Figure 6 illustrates the impact of I_{AM} on the overall system. The total system power follows the general trend of AMTEC power but is slightly higher at the maximum current (~55A). This is due to the fact that TEG benefits from the extra heat rejected by the AMTEC condenser at higher currents. Therefore, when the power starts to drop, the TEG can partially compensate for this decrease. The thermal efficiency of the CHP is relatively high over a large operating envelope because the energy that is not converted to AMTEC electricity can be recovered downstream. The CHP exergy efficiency has, however, its peak value around 60 A because exergy analysis assigns more value to the electrical power output than to the low-grade recovered heat. Hence, the optimum range of 55–60 A is recommended for maximum electrical power output and maximum exergy efficiency. Based on these results, a current of 60 A was proposed as a recommended AMTEC current.

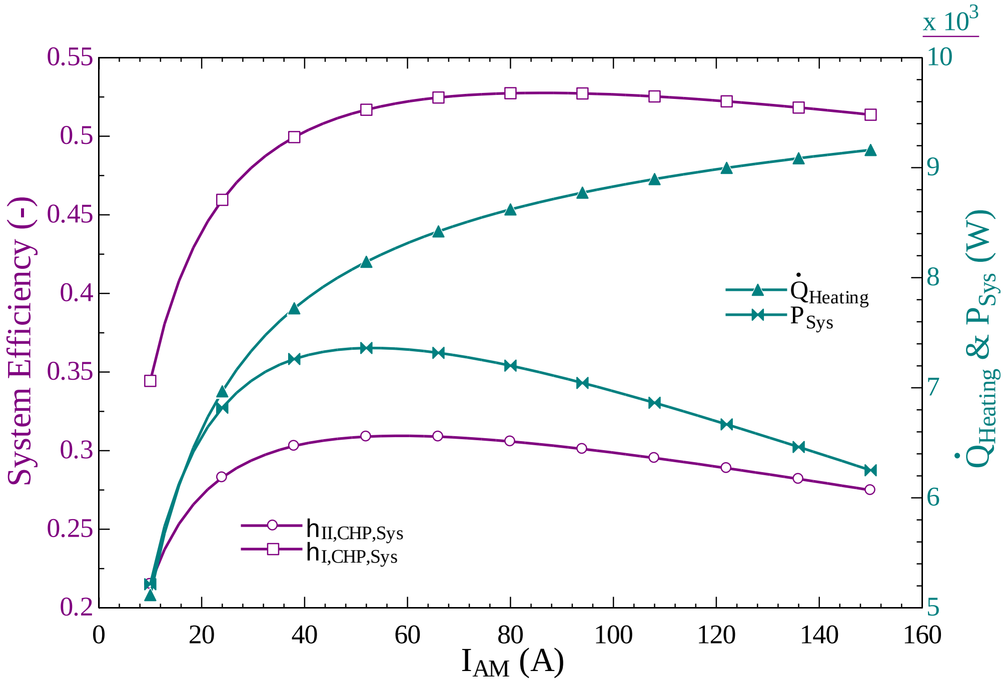

Figure 6 .Effect of AMTEC current on system-level heat and power generation and CHP energy and exergy efficiencies.

- **Effect of AMTEC condenser temperature**

The key thermal coupling parameter between the AMTEC and TEG subsystems is the AMTEC condenser temperature, T_{cond}. There are two opposite effects when increasing T_{cond} has. This decreases AMTEC performance on the one hand by increasing the sodium vapor pressure on the cathode side and, on the other, by reducing the voltage across the BASE elements. On the other hand, it increases the temperature difference and temperature on the hot side of the thermoelectric module, thereby enhancing the TEG performance. These opposing effects are all combined in Figure 7. The changes in CHP energy efficiency are small over the range of T_{cond} investigated, showing that the overall useful energy delivered by the CHP is fairly insensitive to T_{cond}. The CHP exergy efficiency, however, exhibits a distinct peak around 650 K, up to which point the benefit of the improved TEG outweighs the loss of AMTEC output. After this point, the power reduction due to AMTEC starts dominating, and the system's exergetic performance starts to drop. A similar trend is observed for the total electrical power. The TEG gains in power with increasing condenser temperature can compensate for the AMTEC loss of power until around 650 K, beyond which the AMTEC losses are higher than the TEG gains. Therefore, 650 K is regarded as the optimal condenser temperature for AMTEC, providing the best balance between AMTEC performance, TEG recovery, and overall system exergy efficiency.

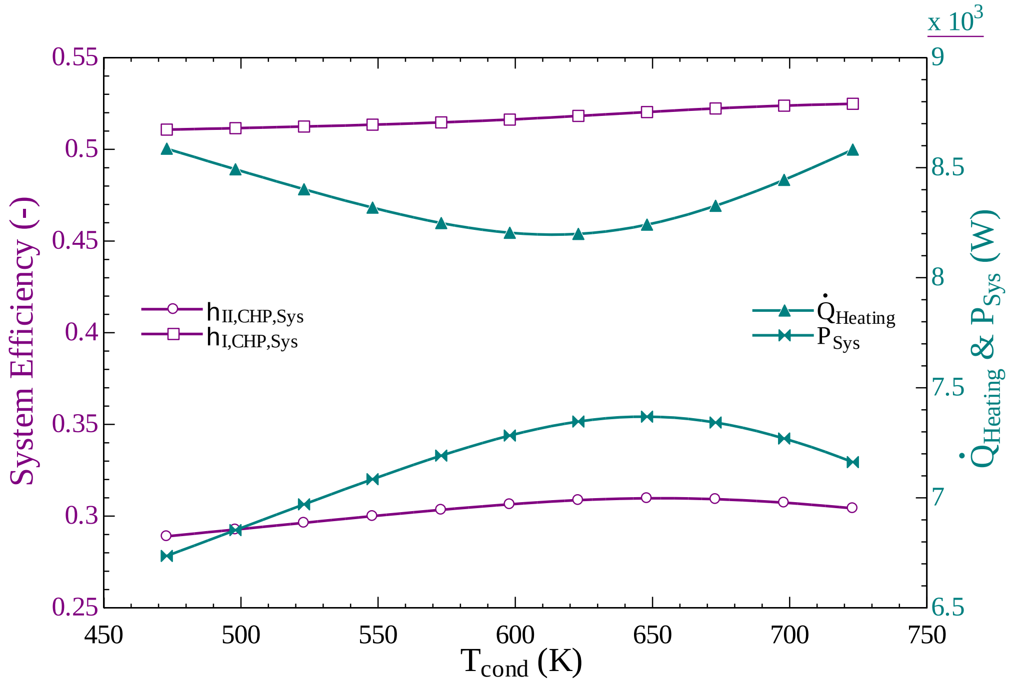

Figure 7. Effect of AMTEC condenser temperature on overall system power generation, recovered heating, and CHP energy and exergy efficiencies.

- **Effect of TEG current**

The TEG current, I_{TEG}, determines the degree of balance between useful thermoelectric power generation and internal resistances. It is shown how it affects the integrated system in Figure 8. The more I_{TEG} increases, the greater the electrical output until the optimum value is achieved. Concurrently, the recovered heat is reduced due to the increased conversion of heat to electricity at the TEG. In the range I_{TEG} studied, the CHP energy efficiency is almost constant. This is because the loss of electrical generation from the optimum is almost offset by a gain of recoverable heat. From a first-law perspective, one can conclude that the TEG current has only a slight influence on the total useful energy production. The CHP exergy efficiency, on the other hand, is more sensitive to I_{TEG}. It peaks at about 9 A, where the TEG has a maximum useful electrical output but has relatively low resistive losses. At lower currents, the temperature difference that can be utilized is smaller, while at higher currents, Joule losses reduce the electrical output. The system's exergy efficiency reduces if the operating conditions are not near this optimum. Thus, 9 A was selected as the suitable TEG current.

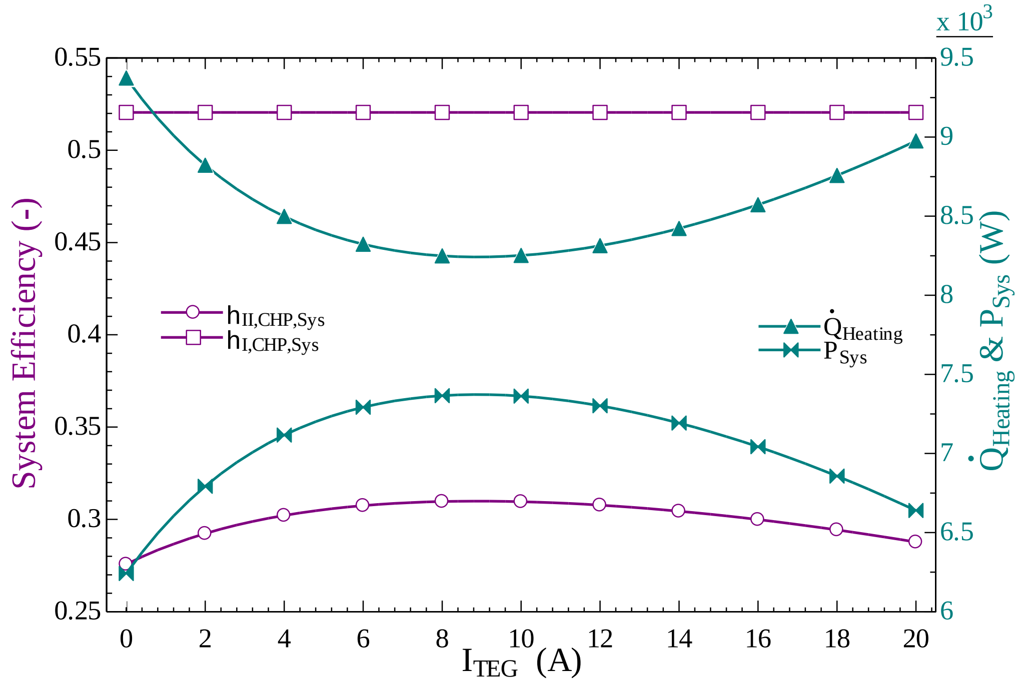

Figure 8. Effect of TEG current on system power generation, recovered heating, and CHP energy and exergy efficiencies.

- **Final recommended operating conditions**

Based on the parametric analysis, the optimum operating conditions of the integrated PDSC–TES–AMTEC–TEG system are summarized in Table 4. These values were chosen as a compromise between electrical generation, useful heat recovery, and exergy efficiency.

Table 4. Recommended operating conditions obtained from the parametric analysis

Parameter	Symbol	Value
Receiver wall temperature	T_W	1220 K
AMTEC current	I_{AM}	60 A
AMTEC condenser temperature	T_{cond}	650 K
TEG current	I_{TEG}	9 A
Heat recovery temperature	$T_{Heating}$	80 °C / 353.15 K

- **Final integrated system performance**

The final performance of the integrated system under the recommended operating conditions is summarized in Table 5. The total electrical power generated by the system is 7372 W, including 6241 W from the AMTEC and 1131 W from the TEG. Moreover, the system can deliver 8242 W of useful heating at 80 °C. The energy efficiency of the electrical energy is 24.75%, and the total CHP energy efficiency is 52.05%, reflecting the advantage of simultaneous use of electrical and thermal power. Considering the second law approach, the electrical and CHP exergy efficiencies are 26.4% and 31.01%, respectively. From these values, it can be seen that the proposed configuration can recover a significant percentage of the input solar energy and also convert a significant percentage of the exergy available into useful products. It is observed that the total exergy destruction rate of the system is 19231 W and that the major sources of irreversibility within the system can be identified.

Table 5. Final integrated system performance under the recommended operating conditions

Parameter	Value
Total electrical power output of the system, P_{Sys}(W)	7372
AMTEC electrical power, P_{AM}(W)	6241
TEG electrical power, P_{TEG}(W)	1131
Useful heating output, $\dot{Q}_{Heating}$(W)	8242
Electrical energy efficiency of the system, $\eta_{I,Ele}^{Sys}$(%)	24.75
Overall CHP energy efficiency, $\eta_{I,CHP}^{Sys}$(%)	52.05
Electrical exergy efficiency of the system, $\eta_{II,Ele}^{Sys}$(%)	26.4
Overall CHP exergy efficiency, $\eta_{II,CHP}^{Sys}$(%)	31.01
Total exergy destruction rate of the system, $\dot{E}x_{D}^{Sys}$(W)	19231

Each of the electrical conversion units contributes as indicated in Figure 9. The AMTEC is the main power-generating component, which is responsible for the generation of around 84.7% of the total electrical power, while the TEG recovers part of the heat rejected from the AMTEC condenser, responsible for about 15.3% of the total electrical power. This reveals that the TEG is not a primary component but an important component in enhancing the overall utilization of the available thermal energy. The same figure also illustrates the distribution of useful system products between electric power and recovered heat, which indicates that the proposed configuration is a CHP system.

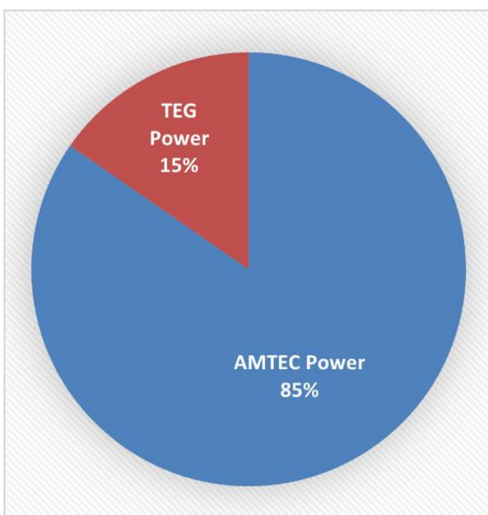

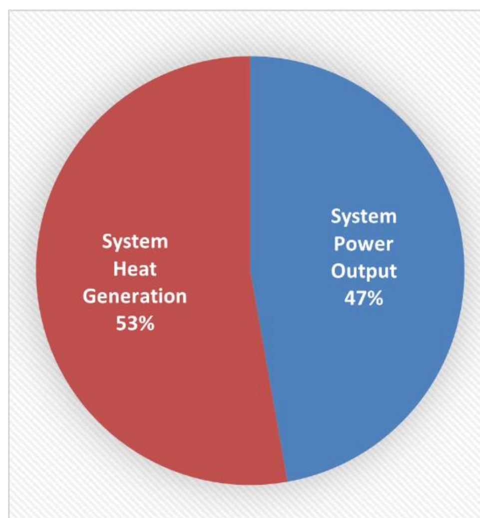

Figure 9. Contribution of AMTEC and TEG to total system electrical power (left) and the share of heat vs. power in total system energy output (right).

The distribution of exergy destruction in the subsystems, as depicted in Figure 10, illustrates the various subsystems involved. Optical losses, receiver thermal losses, and the high exergy content of incoming solar radiation are the principal components of irreversibility in the PDSC. The rest of the exergy destruction takes place in the TES, AMTEC, and TEG. The result suggests that further optimization of the system should be made in the solar collecting/receiving section, with further refinements possible from minimizing AMTEC voltage losses and improving the TEG conversion efficiency.

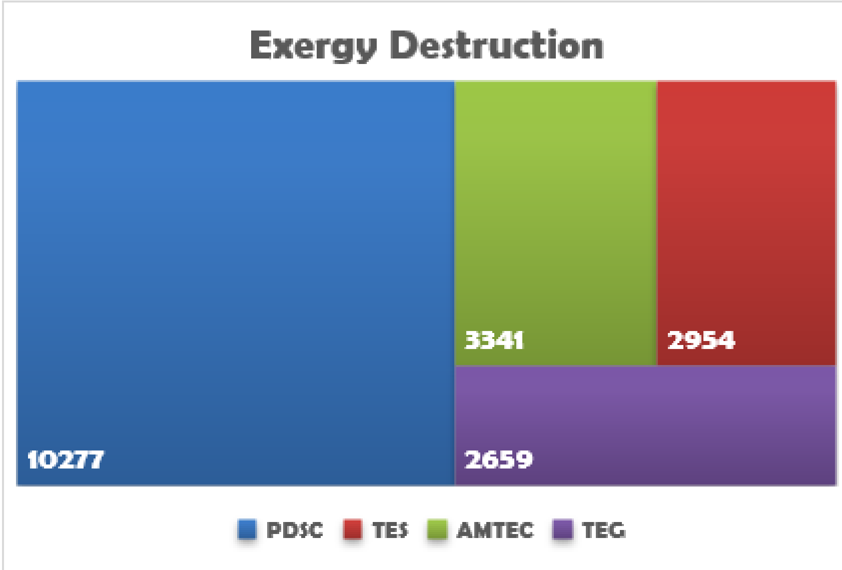

Figure 10. Distribution of subsystem exergy destruction rates in the integrated system.

VI. CONCLUSION

This study provided a thermodynamic analysis of a solid-state solar micro-combined heat and power (CHP) system that includes a parabolic dish solar concentrator, thermal energy storage, an alkali metal thermal-to-electric converter, and a thermoelectric generator. The proposed PDSC–TES–AMTEC–TEG configuration can utilize solar thermal energy in a cascaded manner by generating electricity from high-temperature heat, storing excess solar thermal energy in the TES, and recovering the heat rejected by the AMTEC through the TEG and the heating unit.

The results indicate that the integrated system can produce a total electrical power of 7372 W, with 6241 W provided by the AMTEC, 1131 W provided by the TEG, and 8242 W of useful heating at 80°C. The system has an electrical energy efficiency of 24.75% and an overall combined heat and power (CHP) energy efficiency of 52.05%. The electrical exergy efficiency and overall CHP exergy efficiency are 26.4% and 31.01%, respectively, while the exergy destruction rate is 19231 W.

The results of the exergy analysis show that most of the irreversibility in the process occurs in the solar collection stage, particularly due to optical and thermal losses during high-temperature solar concentration. Further improvements should focus on enhancing the concentrator's optical performance, reducing receiver heat losses, improving the thermal stability of the storage material, and optimizing the thermal coupling between the AMTEC and TEG.

Although the proposed system demonstrates promising thermodynamic performance, its economic feasibility remains an important consideration for practical implementation. The use of specialized components, such as BASE membranes in the AMTEC subsystem, high-temperature containment, and liquid-sodium handling loops, may result in significant capital and maintenance costs. Therefore, a comprehensive techno-economic analysis, including capital expenditure, operating costs, and the levelized cost of energy (LCOE), should be conducted in future work to evaluate the economic competitiveness of the proposed system against other decentralized energy technologies.

The proposed system shows promising potential as a modular solar micro-CHP system based on static power-conversion technologies for decentralized and off-grid energy applications. Future work should involve dynamic simulation, experimental validation, and long-term durability assessment under real operating conditions. In particular, a fully dynamic transient model of the TES charging/discharging process, including PCM phase change evolution and time-dependent heat losses, is recommended for future investigation.

REFERENCES

[1] A. H. Alami, A. G. Olabi, A. Mdallal, A. Rezk, A. Radwan, S. M. A. Rahman, *et al*., "Concentrating solar power (CSP) technologies: Status and analysis," *International Journal of Thermofluids*, vol. 18, 2023, Art. no. 100340, doi: 10.1016/j.ijft.2023.100340.

[2] C. Wu, Y. Zhao, W. Li, J. Fan, H. Xu, Z. Ling, D. Yuan, and X. Zeng, "Concentrated solar thermal power technology and its thermal applications," *Energies*, vol. 18, no. 8, p. 2120, 2025.

[3] O. K. Çakır, Ş. Ela, and M. Ekmekçi, "A comprehensive review of concentrated solar power technologies: Operating principles, efficiency analyses, and energy storage capabilities of tower, parabolic trough, Dish-Stirling, and Fresnel systems," *International Journal of Energy Studies*, vol. 10, no. 4, pp. 1807–1835, 2025.

[4] J. García-Ferrero, R. P. Merchán Corral, J. A. Moctezuma-Hernández, D. Pérez-Gallego, S. Anvari, J. González-Ayala, A. Calvo-Hernández, J. M. Mateos Roco, M. J. Santos, and A. Medina, "Parabolic Dish Collectors for Concentrated Solar Power: A Comprehensive Review on Their Subsystems and Overall Integration," *Energies*, vol. 18, no. 24, p. 6596, 2025.

[5] K. H. Kumar, A. M. Daabo, M. K. Karmakar, and H. Hirani, "Solar parabolic dish collector for concentrated solar thermal systems: A review and recommendations," *Environmental Science and Pollution Research*, vol. 29, 2022, doi: 10.1007/s11356-022-18586-4.

[6] P. Esfanjani, A. Mahmoudi, S. Rashidi, M. S. Valipour, and W. M. Yan, "A review on phase change material's applications in solar parabolic dish collectors," *Journal of Thermal Analysis and Calorimetry*, vol. 149, pp. 13533–13549, 2024, doi: 10.1007/s10973-024-13724-1.

[7] M. Opolot, C. Zhao, M. Liu, S. Mancin, F. Bruno, and K. Hooman, "A review of high temperature (≥ 500 °C) latent heat thermal energy storage," *Renewable and Sustainable Energy Reviews*, vol. 160, 2022, Art. no. 112293, doi: 10.1016/j.rser.2022.112293.

[8] G. Wang, S. Pang, and T. Jiang, "A brief review of liquid heat transfer materials used in concentrated solar power systems and thermal energy storage devices of concentrated solar power systems," *Engineering Reports*, vol. 5, 2023, pp. 1–20, doi: 10.1002/eng2.12576.

[9] M. J. Li, M. J. Li, R. Jiang, S. Du, and X. Y. Li, "Study on the dynamic characteristics of a concentrated solar power plant with the supercritical CO2 Brayton cycle coupled with different thermal energy storage methods," *Energy*, vol. 288, 2024, Art. no. 129628, doi: 10.1016/j.energy.2023.129628.

[10] Z. Kee, J. Coventry, and J. Pye, "Boiling sodium and melting salt: Evaluation and optimisation of a novel solar–thermal system concept," *Applied Thermal Engineering*, vol. 218, 2023, Art. no. 119165, doi: 10.1016/j.applthermaleng.2022.119165.

[11] F. Tohidi, S. Ghazanfari Holagh, and A. Chitsaz, "Thermoelectric Generators: A comprehensive review of characteristics and applications," *Applied Thermal Engineering*, vol. 201, 2022, Art. no. 117793, doi: 10.1016/j.applthermaleng.2021.117793.

[12] W. Peng, J. Gonzalez-Ayala, G. Su, J. Chen, and A. C. Hernández, "Solar-driven sodium thermal electrochemical converter coupled to a Brayton heat engine: Parametric optimization," *Renewable Energy*, vol. 164, pp. 260–271, 2021, doi: 10.1016/j.renene.2020.09.084.

[13] F. Tohidi, S. Khalilarya, A. Chitsaz, and A. Saberi Mehr, "Synergistic integration of alkali metal thermal electric converters and thermoelectric generators: A path to high-efficiency, static conversion of heat to electricity," *Thermal Science and Engineering Progress*, vol. 54, 2024, Art. no. 102879, doi: 10.1016/j.tsep.2024.102879.

[14] W. Peng, J. Gonzalez-Ayala, J. Guo, J. Dong, and Q. Qin, "A two-stage sodium converter coupled to a two-stage TEG: Parametric optimization," *Applied Thermal Engineering*, vol. 229, 2023, Art. no. 120560, doi: 10.1016/j.applthermaleng.2023.120560.

[15] Y. Zhao, Y. Huang, and Z. Chen, “Performance optimization of a solar-driven alkali metal thermoelectric converter coupled to thermally regenerative electrochemical cycles,” *Applied Thermal Engineering*, vol. 219, 2023, Art. no. 119569, doi: 10.1016/j.applthermaleng.2022.119569.

[16] S. Y. Wu, L. Xiao, Y. Cao, and Y. R. Li, “A parabolic dish/AMTEC solar thermal power system and its performance evaluation,” Applied Energy, vol. 87, no. 2, pp. 452–462, 2010, doi: 10.1016/j.apenergy.2009.08.041.

[17] J.-M. Tournier and M. El-Genk, “Design optimization of high-power, liquid anode AMTEC,” in AIP Conference Proceedings, vol. 654, 2003, pp. 740–750, doi: 10.1063/1.1541362.

[18] M. Liao, Z. He, C. Jiang, X. Fan, Y. Li, and F. Qi, “A three-dimensional model for thermoelectric generator and the influence of Peltier effect on the performance and heat transfer,” Applied Thermal Engineering, vol. 133, pp. 493–500, 2018, doi: 10.1016/j.applthermaleng.2018.01.080.

[19] E. Bellos and C. Tzivanidis, “Optimum design of a solar ejector refrigeration system for various operating scenarios,” Energy Conversion and Management, vol. 154, pp. 11–24, 2017, doi: 10.1016/j.enconman.2017.10.057.

[20] J.-M. Tournier, M. S. El-Genk, M. Schuller, and P. Hausgen, “An analytical model for liquid-anode and vapor-anode AMTEC converters,” in Space Technology and Applications International Forum (STAIF-97), 1997, pp. 1543–1552, doi: 10.1063/1.51977.

[21] M. A. Ryan, “Lifetimes of AMTEC electrodes: Molybdenum, rhodium-tungsten, and titanium nitride,” in AIP Conference Proceedings, vol. 504, 2000, pp. 1377–1382, doi: 10.1063/1.1290954.

[22] S. Shittu, G. Li, X. Zhao, X. Ma, Y. G. Akhlaghi, and Y. Fan, “Comprehensive study and optimization of concentrated photovoltaic-thermoelectric considering all contact resistances,” Energy Conversion and Management, vol. 205, Art. no. 112422, 2020, doi: 10.1016/j.enconman.2019.112422.